RESEARCH ARTICLE

Correspondence to:
S. Park,
sungsup@snu.ac.kr;
S.-J. Kim,
seongjkim@kopri.re.kr

Impact of detrained cumulus on climate simulated by the Community Atmosphere Model Version 5 with a unified convection scheme

Sungsu Park[1] , Eun-Hyuk Baek[2], Baek-Min Kim[2] , and Seong-Joong Kim[2]

[1]School of Earth and Environmental Sciences, Seoul National University, Seoul, South Korea, [2]Korea Polar Research Institute, Incheon, South Korea

Abstract Cumulus elements generated by detraining convective condensate–detrained cumulus–are added to the Community Atmosphere Model Version 5 (CAM5) combined with a Unified Convection Scheme (UNICON). Instead of evaporating convective liquids detrained into clear portions, we diagnosed a new detrained cumulus that is horizontally nonoverlapped with cumulus and stratus in each layer by assuming a steady state balance between the detrainment rate of cumulus condensates and the dissipation rate of detrained condensates by entrainment mixing with environmental air. The addition of detrained cumulus was found to substantially improve the simulation of low-level clouds and the associated short-wave cloud radiative forcing, particularly in the subtropical trade cumulus regime. In addition to the mean climate, successful simulations of the diurnal cycle of precipitation, Madden-Julian Oscillation, and Kelvin wave were also well maintained.

1. Introduction

Clouds are an important but uncertain feature of the climate system. Due to their diverse impacts on the global climate with complex interactions, clouds have been the focus of various research during the recent few decades both in the observation and the modeling communities [e.g., *Ramanathan et al.*, 1989;, *Hahn and Warren*, 1999; *Bony and Dufresne*, 2005; *Park et al.*, 2014]. From the macrophysical and dynamical points of view, clouds can be grouped into two categories, cumulus and stratus. Cumulus has a small horizontal but large vertical extent, while stratus has a large horizontal but small vertical extent. When convective condensates are detrained from cumulus at their neutral buoyancy levels, a third type of cloud, detrained cumulus, can be generated. Detrained cumulus plays an important role in various aspects of climate processes, such as climate sensitivity associated with cirrus and stratocumulus [*Lindzen et al.*, 2001; *Hartmann and Michelsen*, 2002; *Ramanathan and Collins*, 1991; *Medeiros et al.*, 2008] and the enhanced persistence of sea surface temperature (SST) through positive cloud-SST radiative feedback [*Park et al.*, 2005, 2006].

Instead of representing individual stratus and detrained cumulus, modern cloud schemes originally proposed by *Smith* [1990] and *Tiedtke* [1993], as well as their successors, attempted to parameterize the combined properties of two distinctively different stratus and detrained cumulus with a single set of diagnostic or prognostic equations. Although its macrophysical properties resemble those of stratus with a large horizontal area, the thermodynamic properties of detrained cumulus are not necessarily correlated with those of the preexisting stratus. In contrast to stratus parameterized by the local grid-mean scalars at a single height, the thermodynamic properties of detrained cumulus are determined by the vertical integration of complex physical processes (i.e., nonlocal processes). In addition, detrained cumulus is likely to have a vertical overlap structure (e.g., maximum overlap), largely different from that of stratus (e.g., maximum-random overlap depending on the vertical separation distance between two stratus layers). Due to these contrasting natures, it is more reasonable to parameterize detrained cumulus separately from stratus.

As a first step toward developing a comprehensive cloud scheme taking into account individual cumulus, stratus, and detrained cumulus, we implement a simple method diagnosing the detrained cumulus fraction into the CAM5 [*Park et al.*, 2014] combined with UNICON [*Park*, 2014a] and show its impacts on the global climate.

2. Convective Detrainment With UNICON

Park [2014a] developed a UNICON and tested its global performance within CAM5. UNICON is designed to simulate all dry-moist, forced-free, and shallow-deep convection within a single framework in a seamless, consistent, and unified manner, replacing the CAM5 shallow convection [*Park and Bretherton*, 2009] and deep convection schemes [*Zhang and McFarlane*, 1995]. *Park* [2014b] showed that UNICON successfully simulates various atmospheric variabilities (e.g., the diurnal cycle of precipitation, Madden-Julian Oscillation (MJO) [*Madden and Julian*, 1971]) without degrading the mean climate. It diagnoses vertical profiles of the cumulus fraction and in-cumulus condensates, as well as the convective detrainment rate. In this study, we made the following three minor modifications to the UNICON used in *Park* [2014b]: (1) the conservative scalars of the convective updraft plumes at the top of the PBL are explicitly calculated without assuming a rough similarity to the mean bulk properties of the noncold pool area; (2) a refined numerical scheme is used in computing the production (evaporation) rate of convective precipitation within convective updraft (downdraft); and (3) a few tuning parameters are adjusted within allowable ranges to obtain the global energy balance at the top of the atmosphere (TOA). Essentially, the fundamental physics of the UNICON used in this study is identical to those of the original UNICON of *Park* [2014a], except the revised treatment of detrained convective condensates explained below.

The CAM5 cloud macrophysics scheme developed by *Park et al.* [2014] assumes that detrained convective condensates are randomly distributed within each layer and convective liquids detrained into the clear portion are immediately evaporated until the clear portion is saturated (see Figure1a). Since the stratus fraction in CAM5 is a function of the environmental relative humidity, $\tilde{U}$ (i.e., the stratus fraction is formed when $\tilde{U}$ is larger than a certain critical U_c, say, 0.9), the stratus fraction may increase in response to the evaporative increase of $\tilde{U}$ (dashed line in Figure 1a). However, in regimes where convective condensates are frequently detrained, $\tilde{U}$ was found to be much lower than U_c, such that the stratus fraction does not increase even after the evaporation of detrained convective liquids. In order to address this issue, following the approaches of *Tiedtke* [1993] and *Teixeira and Kim* [2008], we hereby diagnose additional cloud fractions generated by convective condensates detrained into the clear portion as follows (*detrained cumulus, A_{dc}* in Figure 1b):

$$A_{dc} = (1 - A_{cu} - A_{st}) \cdot \left[\frac{M_{det} \cdot (q_{l,det} + q_{i,det})}{M_{det} \cdot (q_{l,det} + q_{i,det}) + c_{ero} \cdot \tilde{q}_s \cdot (1 - \tilde{U}) \cdot (\Delta p/g)} \right], \qquad (1)$$

where A_{cu} is a cumulus fraction that is a function of the mass flux and vertical velocity of convective updraft plumes, i.e., $A_{cu} = \hat{M}/(\rho\hat{w})$, where ρ is air density; A_{st} is a stratus fraction that is a function of environmental relative humidity $\tilde{U}$; M_{det} is detrained convective mass flux; $q_{l,det}$ and $q_{i,det}$ are the liquid and ice masses of detrained convective condensates, respectively; $\tilde{q}_s$ is the saturation specific humidity of the environment;
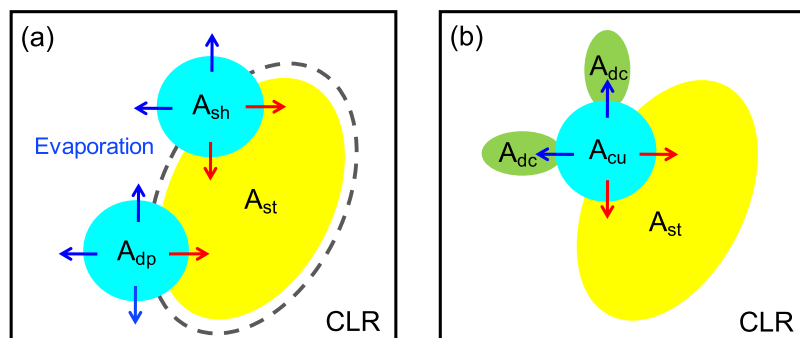

Figure 1. Schematic diagrams illustrating the treatment of detrained convective condensates. (a) CAM5: Both shallow cumulus (with a fractional area A_{sh}) and deep cumulus (A_{dp}) detrain convective condensates into the preexisting stratus (A_{st}, red arrows) and the clear portion (CLR, blue arrow). Convective liquids detrained into the clear portion are instantaneously evaporated until the clear portion is saturated. A_{st} increases if the environmental relative humidity after evaporation of detrained convective liquids increases above the critical relative humidity (dashed black line). (b) UNICON: A single cumulus (A_{cu}) detrains convective condensates into the environment. Instead of evaporating detrained convective liquids, a new detrained cumulus fraction is diagnosed (A_{dc}, green shading) as an increasing function of the amount of convective condensates detrained into the clear portion and the environmental relative humidity. The original UNICON of *Park* [2014b] (i.e., P2014 in the text) features the same treatment of detrained convective condensates as CAM5, except that P2014 has a single A_{cu} instead of separate A_{sh} and A_{dp}.

Δp is the pressure thickness of the model layer; and c_{ero} is a tunable erosion coefficient which is set to 10^{-6} $[s^{-1}]$. This formula is obtained by assuming a steady state balance between the production of detrained cumulus by convective detrainment and the dissipation of detrained cumulus due to entrainment mixing with environmental air. The resulting total cloud fraction in each layer is $A_{tot}=A_{cu}+A_{st}+A_{dc}$ where $0 \leq A_{tot} \leq 1$. Similar to the cumulus and stratus, this approach guarantees that detrained cumulus is not empty, i.e., it always has a nonzero condensate mass [*Park et al.*, 2014]. This formula indicates that A_{dc} increases as the amount of detrained convective condensates increases and as the environment becomes more moist. The first factor on the r.h.s. implies that only the convective condensates detrained into the clear portion can generate an additional detrained cumulus fraction; however, convective condensates detrained into the existing stratus do not generate any additional cloud fraction.

In all the existing convection schemes with a quasi-conserved plume approximation, condensates within cumulus are not parts of the prognosed grid-mean thermodynamic scalars, but condensates within detrained cumulus and stratus contribute to the grid-mean tendencies. Because a separate prognostic equation for the condensate of detrained cumulus has not been implemented yet, we only prognose the combined internal properties of stratus and detrained cumulus. Similar to CAM5, the radiation scheme in the revised UNICON uses a single total cloud fraction (A_{tot}) and homogeneous in-cloud condensate $\hat{q}_{l,tot}=(A_{cu}\hat{q}_{l,cu}+A_{st}\hat{q}_{l,st}+A_{dc}\hat{q}_{l,dc})/A_{tot}$ and $\hat{q}_{i,tot}=(A_{cu}\hat{q}_{i,cu}+A_{st}\hat{q}_{i,st}+A_{dc}\hat{q}_{i,dc})/A_{tot}$) where $\hat{q}_l$ and $\hat{q}_i$ denote in-cloud liquid and ice condensate masses, respectively. In this manner, the radiation scheme takes into account detrained cumulus. Detrained convective condensates also precipitates, such that they interfere with the model water budget as well as the radiation budget.

In the following section, we will compare a set of three UNICON simulations with CAM5 and observations. The simulation with the original UNICON of *Park* [2014b] will be referred to as P2014. The revised UNICON that incorporates the detrained cumulus and the abovementioned three minor modifications into P2014 will be simply referred to as UNICON. In order to isolate the impacts of detrained cumulus from those of three minor modifications that include the adjustment of a few tuning parameters, we performed an additional simulation, named NoAdc (e.g., no A_{dc}) by removing the detrained cumulus from the revised UNICON. CAM5 and P2014 feature an identical treatment of detrained convective condensates as shown in Figure 1a, except that P2014 has a single cumulus fraction (A_{cu}) instead of separate shallow cumulus (A_{sh}) and deep cumulus fraction (A_{dp}).

3. Results

3.1. Global-Annual Mean Statistics

As a first step toward the evaluation of the impact of detrained cumulus on the mean climate, we show a Taylor diagram (Figure 2) [*Taylor*, 2001] summarizing various statistics for global simulations compared with observations. Similar to *Park* [2014b], we conducted an Atmospheric Model Inter-comparison Project (AMIP) simulation forced by the observed inter-annual SST and sea-ice fraction with an annual cycle for 27 years from January 1979 to February 2006 at a horizontal resolution of 1.9° latitude x 2.5° longitude with 30 vertical layers. The global performance of UNICON is similar to that of CAM5 and better than that of P2014 and NoAdc with a relative spatiotemporal root-mean-square error (RMSE) of 0.748, with respect to CCSM3.5: 0.754 for CAM5, 0.786 for P2014, and 0.809 for NoAdc. Compared to CAM5 and P2014, the largest improvement of UNICON is in SWCF and land rainfall. One notable degradation is the amplification of the spatiotemporal variability of longwave cloud radiative forcing (LWCF) in association with the positive biases of LWCF over the tropical deep convection regions. Further tunings could have been made to address this bias, e.g., by changing the critical diameter of ice crystals at which stratus ice condensates start to convert into snow. However, we did not perform additional tunings in order to evaluate the isolated impact of detrained cumulus as much as possible.

3.2. SWCF and Low-Level Cloud

Figure 3 shows the biases of annual-mean SWCF against the observation and the differences of low-level cloud fraction (CLDLOW) between the simulations. Compared to CAM5, P2014 substantially improved the simulation of SWCF in the tropical deep convection region and Southern Hemispheric circumpolar region along 60°S (Figures 3c and 3d), which was attributed to the smaller cumulus fraction and the treatment of wet scavenging of in-cumulus aerosols by convective precipitation [*Park*, 2014b]. The improved SWCF over
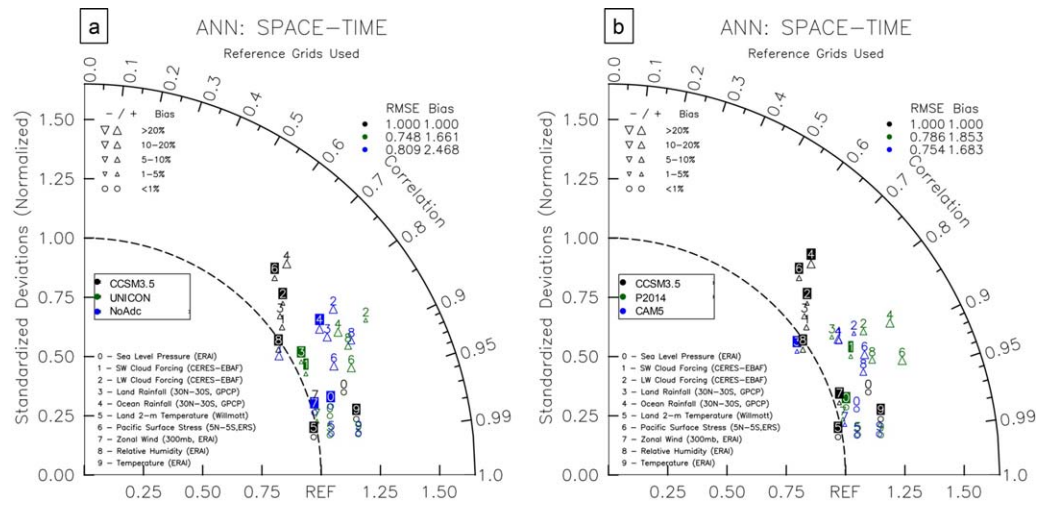
Figure 2. Space-time Taylor diagrams showing the global performance of (a) UNICON (green) and NoAdc (blue), and (b) P2014 (green) and CAM5 (blue) relative to CCSM3.5 (black) against observations made according to the correlation and standardized deviation of 10 semiindependent climate variables. The RMSE (root-mean-square error) is the average of relative RMSE of a simulated individual variable against the observation with respect to the RMSE of CCSM3.5. The Bias is the average of relative mean of an individual variable with respect to CCSM3.5. See *Park* [2014b] for more details.

the Southern Hemispheric circumpolar region may help to remedy the longstanding bias of the double Intertropical Convergence Zone in GCM [*Hwang and Frierson*, 2013]. Over the eastern subtropical trade wind regimes, however, P2014 tends to simulate more clouds upstream (negative bias of SWCF) but less clouds downstream (positive bias of SWCF) than the observation. These biases are substantially reduced in UNICON that simulates more CLDLOW in the downstream portion than P2014 (Figures 3a, 3c, and 3g). The RMSE of SWCF decreases from 15.6 (Wm^{-2}) in CAM5 to 11.7 in P2014 and 9.4 in UNICON.

The isolated impacts of detrained cumulus on CLDLOW separated from those of the tunings and other minor modifications are shown in Figure 3f. Detrained cumulus substantially increases marine CLDLOW particularly over the eastern subtropical oceans, with a global mean increase of ΔCLDLOW = 10.2%. With additional tunings that decrease CLDLOW over the oceans as shown in Figure 3e (e.g., increase in critical relative humidity U_c for the low-level cloud fraction), UNICON roughly restored P2014's global energy balance at TOA. However, systematic regional differences exist in the simulated CLDLOW between UNICON and P2014 (Figure 3g). The maximum ΔCLDLOW over the subtropical trade wind regime shown in Figures 3g and 3h is collocated over an area where the surface observed climatological frequencies of CL8 (cumulus under stratocumulus) and CL4 (stratocumulus formed by the spreading out of cumulus) are maximum [*Hahn and Warren*, 1999; *Norris*, 1998]. This implies that our simulated detrained cumulus reflects the observed characteristics of the detrained cumulus well. CL is a low-level cloud code used by surface observers defined by *WMO* [1975]; see also *Park and Leovy* [2004]. It is interesting to note that even though it is a convection scheme, UNICON also improved the simulation of Arctic clouds. Presumably, this is partly because UNICON is designed to simulate extra-tropical convection as well as tropical convection [*Park*, 2014a] and convective activities are frequently observed in the Arctic area in association with the intrusion of synoptic storms into the Arctic area.

3.3. LWP and IWP From Individual Cloud Types
Figure 4 shows the contribution of stratus, cumulus, and detrained cumulus to the total cloud LWP (TGCLDLWP) during DJF and JJA. Stratus LWP mainly exists in the midlatitudes, eastern subtropical stratocumulus decks, and over China throughout the year and also over the Arctic during JJA. In the midlatitudes, the summer hemisphere has more stratus than the winter hemisphere, and stratus is particularly abundant in China during DJF. Cumulus LWP mostly exists in the tropical deep convection regions and to a less extent, in the trade cumulus regimes. Most of the detrained cumulus LWP exists over the eastern subtropical stratocumulus and trade cumulus regimes, as well as the midlatitude regions. The global mean LWP of detrained cumulus is similar to that of cumulus, which is about 25% of stratus LWP. Over the eastern subtropical oceans, the maximum LWP of detrained cumulus seems to be collocated with that of stratus, which
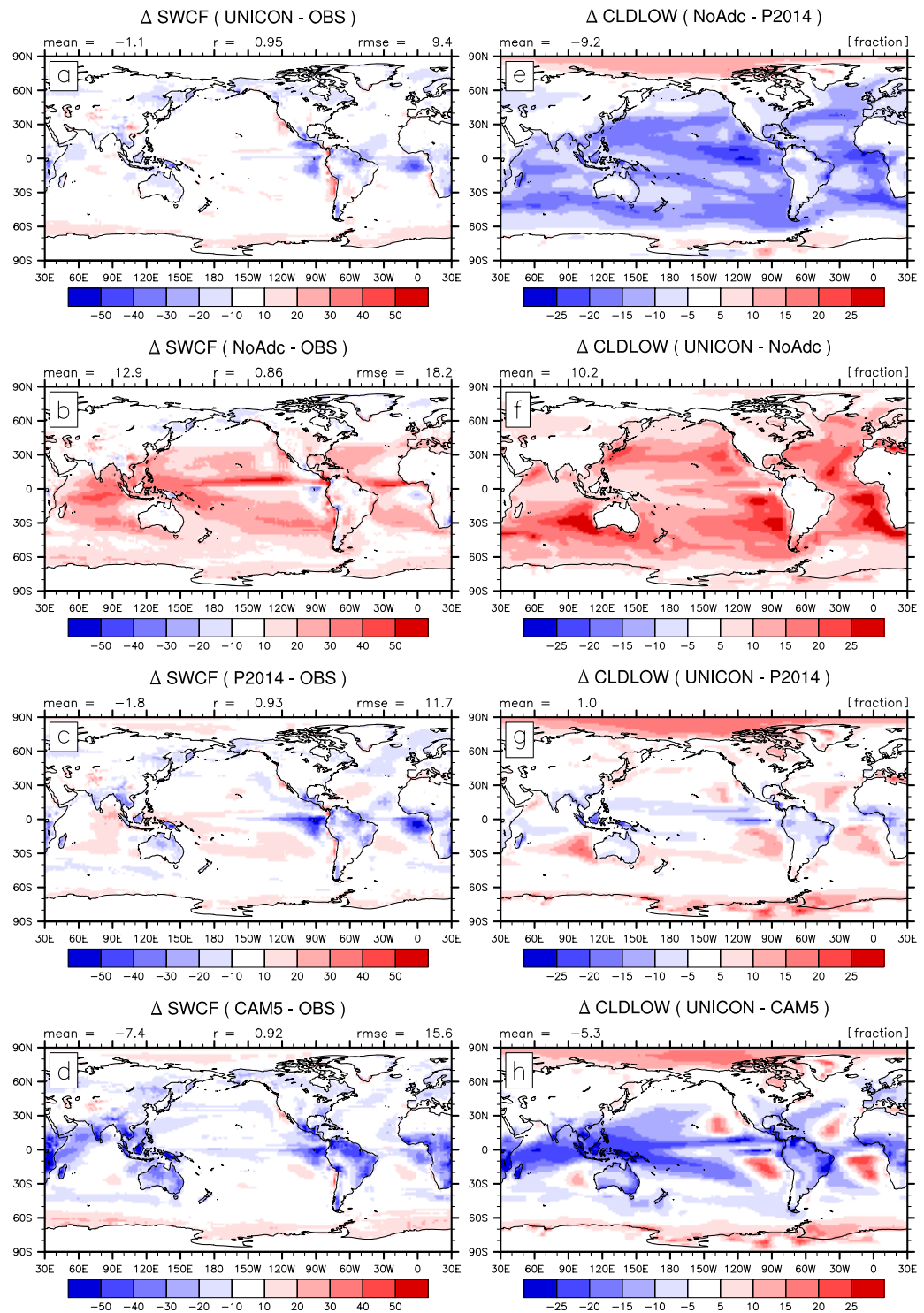
Figure 3. Biases of annual-mean shortwave cloud radiative forcing (SWCF, [W m^{-2}]) against the CERES-EBAF observation during March 2000 to February 2010 from (a) UNICON, (b) NoAdc, (c) P2014, and (d) CAM5, and (e–h) the difference of annual-mean low-level cloud fraction (CLDLOW, [%]) between the simulations. In Figures 3a–3d, the difference of the area-weighted global-mean value (*mean*), global pattern correlation (*r*) and *rmse* between the simulation and the observation are denoted at the top of individual plots. In Figures 3e–3h, the difference of the area-weighted global-mean value (*mean*) is denoted at the top left of individual plots.

is somewhat unusual since the maximum cumulus fraction in nature is observed further downstream from the maximum stratus fraction. We note that UNICON is designed to simulate not the observed cumulus but the relative nonlocal subgrid plumes with respect to the grid-mean flow, such that it is active in the marine
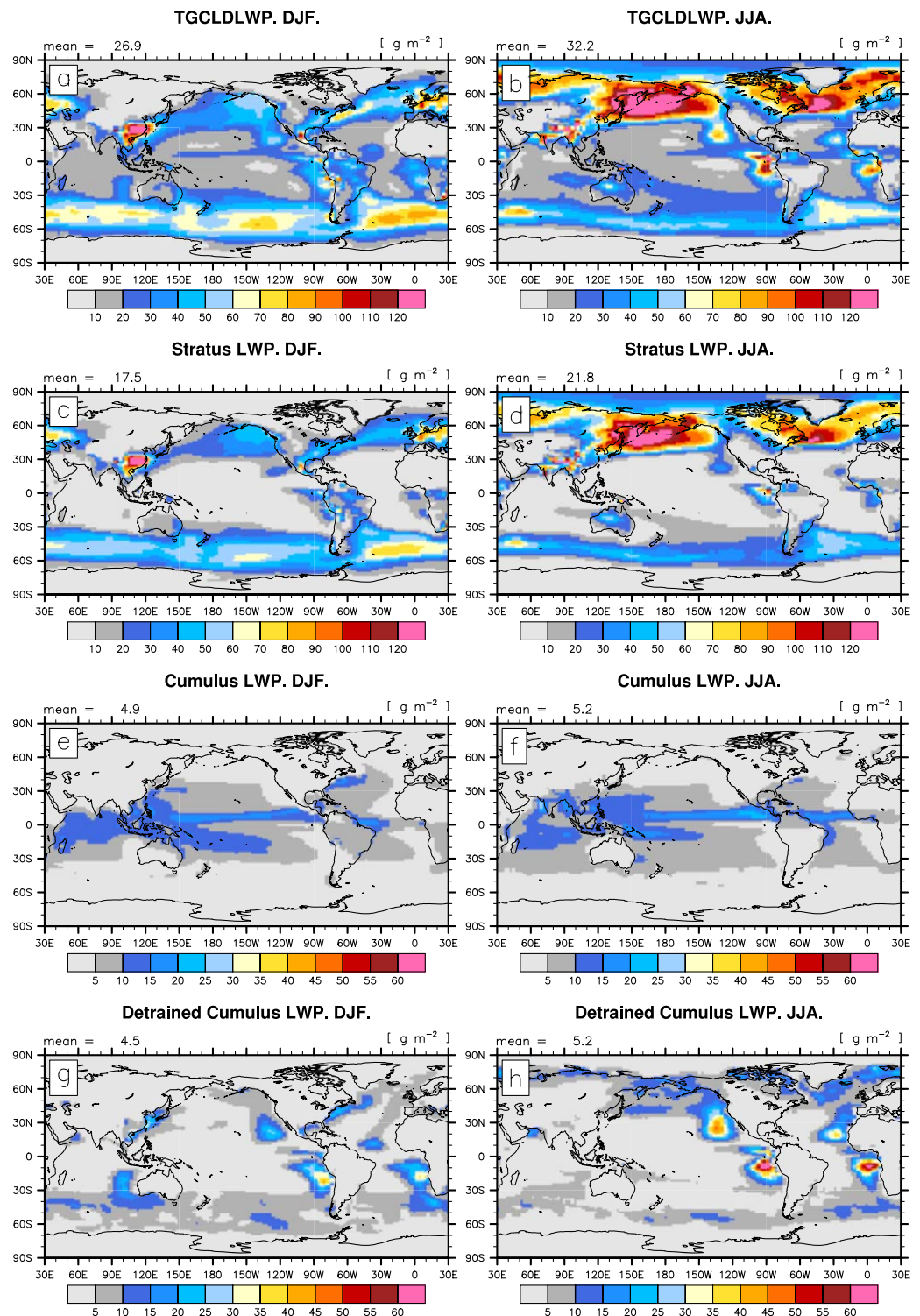
Figure 4. UNICON-simulated column-integrated grid-mean LWC during (left) DJF and (right) JJA from (a, b) all types (stratus + cumulus + detrained cumulus) of clouds (TGCLDLWP); (c, d) stratus; (e, f) cumulus; and (g, h) detrained cumulus. The area-weighted global mean value is denoted at the top left of individual plots.

stratocumulus deck as well as in the trade cumulus regimes [see *Park*, 2014b, Figure 2]. As shown in Figure 8, detrained cumulus plays an important role in the downstream extension of the stratocumulus deck in the trade cumulus regimes.
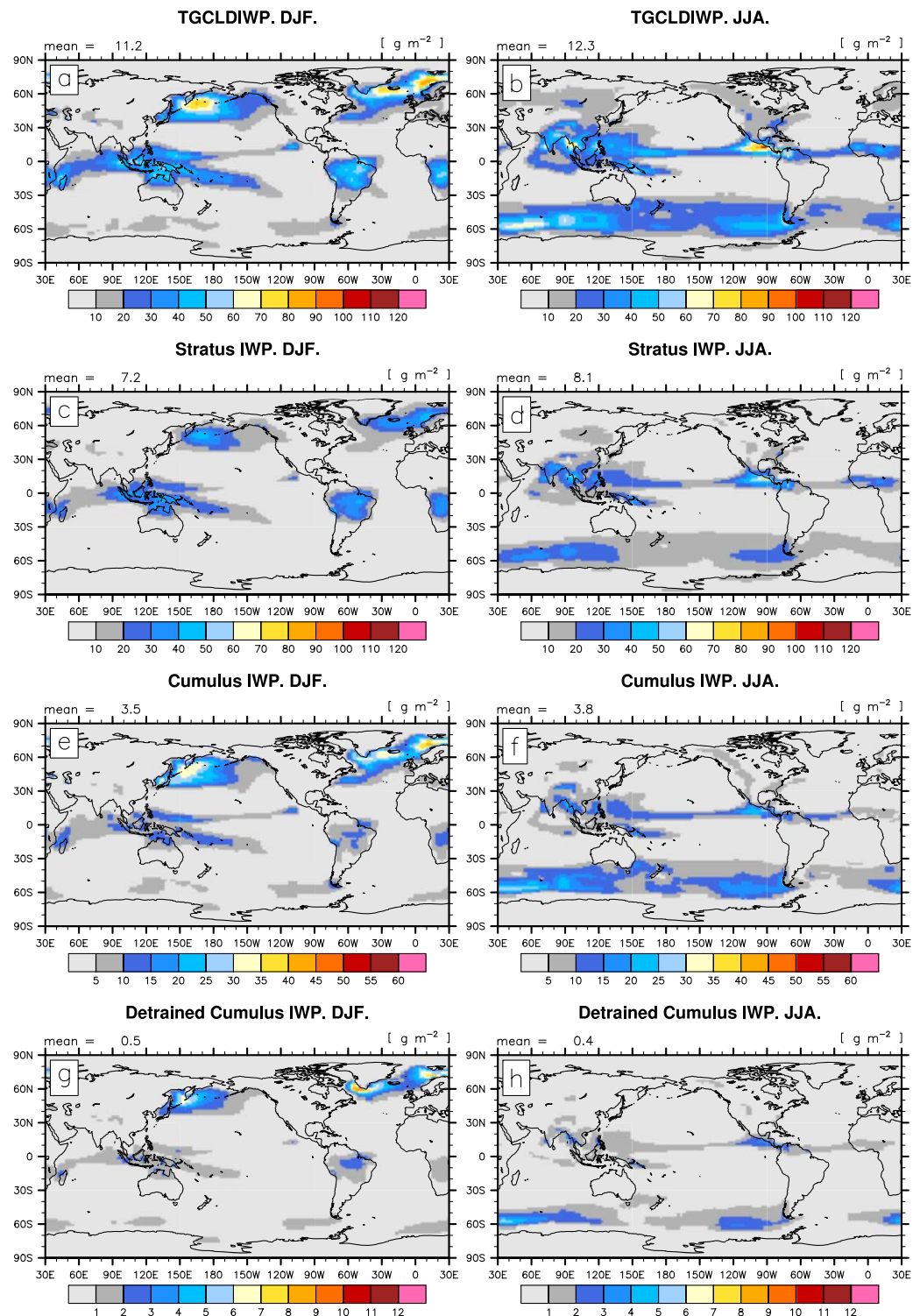
Figure 5. UNICON-simulated column-integrated grid-mean IWC during (left) DJF and (right) JJA from (a, b) all types (stratus + cumulus + detrained cumulus) of clouds (TGCLDIWP); (c, d) stratus; (e, f) cumulus; and (g, h) detrained cumulus. The area-weighted global mean value is denoted at the top left of individual plots.

Figure 5 shows the contribution of stratus, cumulus, and detrained cumulus to the total cloud IWP (TGCLDIWP) during DJF and JJA. In contrast to stratus LWP, the winter hemisphere has more stratus IWP than the summer hemisphere in the midlatitudes, and an additional maximum of stratus IWP exists in the
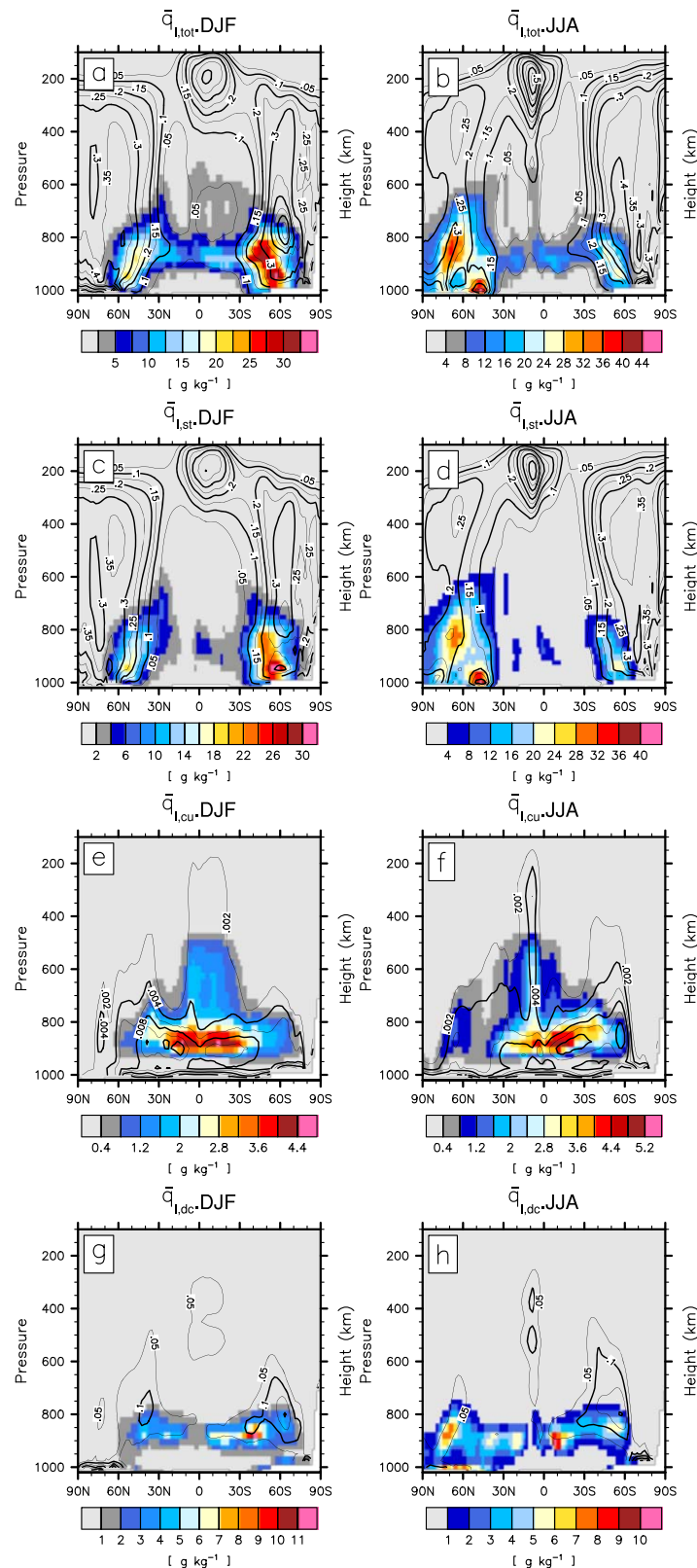
Figure 6. UNICON-simulated zonal-mean cross sections of grid-mean cloud liquid condensate masses (color shading (g kg^{-1})) and cloud fractions (solid lines (fraction)) for (top) total cloud (A_{tot}), (the second row) stratus (A_{st}), (the third row) cumulus (A_{cu}) and (bottom) detrained cumulus (A_{dc}) during (left) DJF and (right) JJA.

tropical deep convection region. The global mean IWPs of cumulus and detrained cumulus are about a half and less than 10% of stratus IWP, respectively. Overall, the spatial patterns of cumulus and detrained cumulus IWP are quite similar to that of stratus. As mentioned earlier, UNICON is designed to simulate extratropical convection as well as tropical convection, so that the IWPs from stratus, cumulus, and detrained cumulus similarly have the maximum over winter midlatitude storm track regions.

3.4. Zonal-Mean Cross Sections of Cloud Properties

Figure 6 shows UNICON-simulated zonal-mean cross sections of grid-mean LWC of the total cloud ($\overline{q}_{l,tot}$), stratus ($\overline{q}_{l,st}$), cumulus ($\overline{q}_{l,cu}$) and detrained cumulus ($\overline{q}_{l,dc}$) with corresponding cloud fractions (A_{tot}, A_{st}, A_{cu}, A_{dc}) during DJF and JJA. Similar plots for grid-mean IWC are shown in Figure 7. The properties of a single merged cloud provided to the radiation scheme are A_{tot} and $\hat{q}_{l,tot} = \overline{q}_{l,tot}/A_{tot}$ and $\hat{q}_{i,tot} = \overline{q}_{i,tot}/A_{tot}$. Both CAM5 and UNICON compute $A_{st} = \max(A_{l,st}, A_{i,st})$ where the liquid stratus fraction $A_{l,st}$ is a function of grid-mean relative humidity (RH) over water, and the ice stratus fraction $A_{i,st}$ is a function of grid-mean RH over ice and additionally, $\overline{q}_{i,st}$ [Park et al., 2014]. As a result, the pattern of A_{st} resembles the patterns of grid-mean RH (not shown) and $\overline{q}_{i,st}$.

Similar to CAM5 [Park et al., 2014], UNICON simulates a maximum $\overline{q}_{l,st}$ at around 875 hPa along 45°N/S. In the midlatitudes during summer, nonzero $\overline{q}_{l,st}$ extends down to the surface, indicating the formation of advection fog. UNICON simulates the maxima $\overline{q}_{i,st}$ in the tropical upper troposphere and
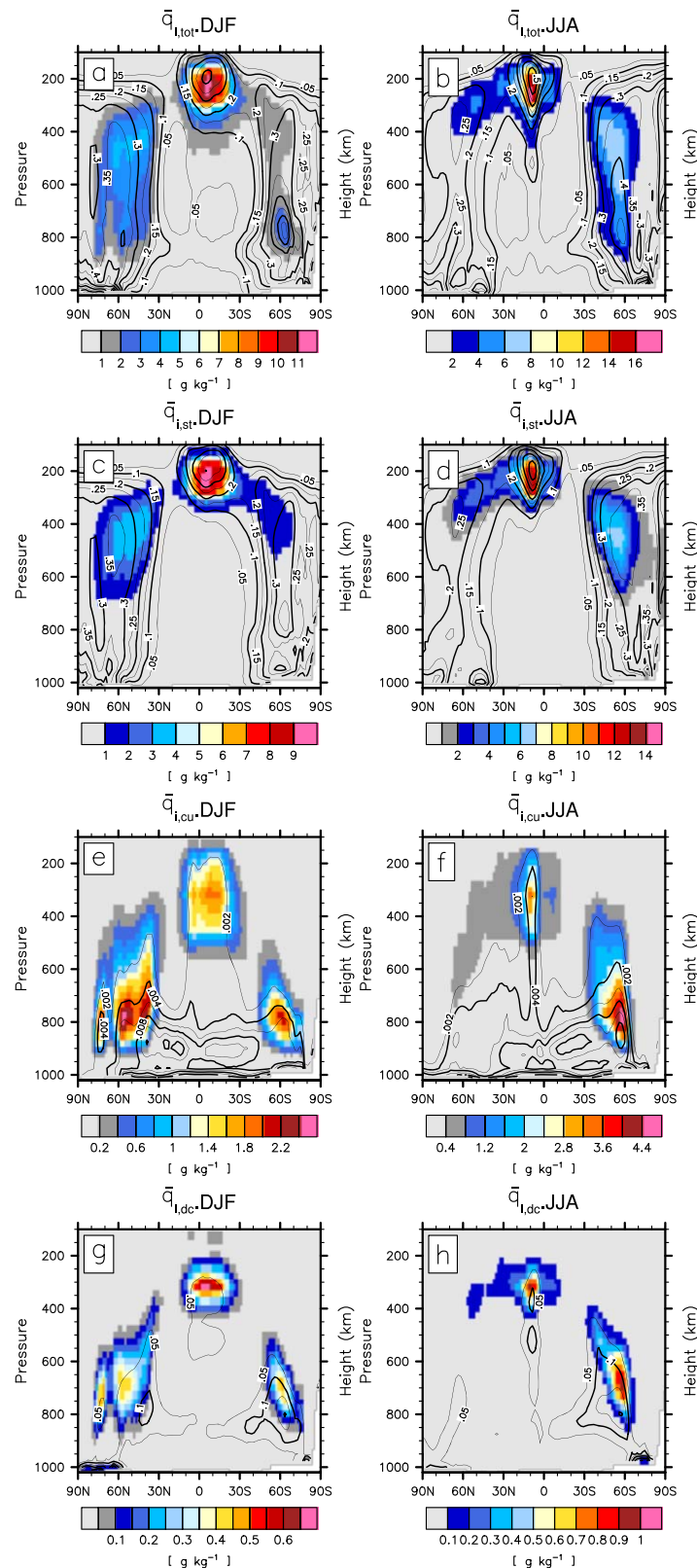
Figure 7. UNICON-simulated zonal-mean cross sections of grid-mean cloud ice condensate masses (color shading (g kg^{-1})) and cloud fractions (solid lines (fraction)) for (top) total cloud (A_{tot}), (the second row) stratus (A_{st}), (the third row) cumulus (A_{cu}) and (bottom) detrained cumulus (A_{dc}) during (left) DJF and (right) JJA.

the midlatitude storm track regions during boreal winter. Cumulus shows a maximum $\overline{q}_{l,cu}$ in the tropical and subtropical lower troposphere and a maximum $\overline{q}_{i,cu}$ in the tropical upper troposphere and the midlatitude storm track regions. As expected, the pattern of detrained cumulus is similar to that of cumulus both in terms of cloud fraction and grid-mean condensate amount. Over the Arctic area, detrained cumulus shows a maximum cloud fraction during DJF and a maximum grid-mean liquid condensate mass during JJA.

3.5. Cross Sections in the Marine Subtropical Stratocumulus Deck

In order to obtain insights into the physical processes responsible for the improved simulation of low-level cloud over the downstream portion of the eastern subtropical trade wind regions, we plotted the cross-sections of grid-mean potential temperature (θ) and cloud properties, the grid-mean detrainment rate of convective condensates (D) and the grid-mean net condensation rate (Q) along 20°S from coastal Peru to the South Pacific Convergence Zone during September, October, and November. The plots are shown in Figure 8. A_{tot} is total cloud fraction, q_l is the grid-mean cloud LWC, and M is the convective updraft mass flux. All simulations successfully simulated the stratocumulus deck at the top of the well-mixed PBL near the coast, the development of decoupled PBL with a horizontally extended stratocumulus deck at the top of the cumulus layer further offshore, and the dissipation of the stratocumulus deck further downstream. The development of the decoupled PBL can be identified from a stably stratified cumulus layer above the surface-based well-mixed
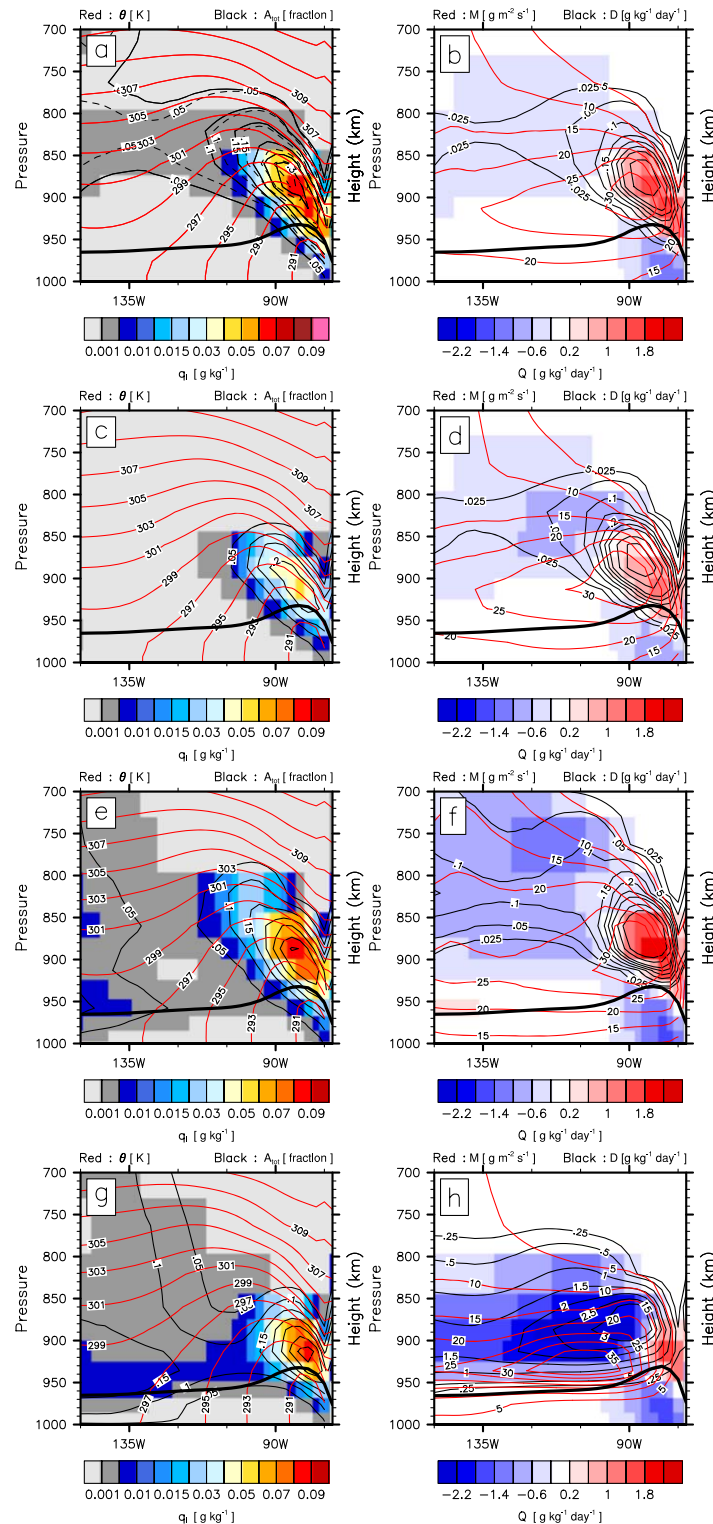
Figure 8. Vertical cross sections of (a, c, e, g) grid-mean potential temperature $\overline{\theta}$ (red line), total cloud fraction A_{tot} (black line), and grid-mean $\overline{q}_l$ (color) and (b, d, f, h) convective updraft mass flux M (red line), grid-mean detrainment rate of convective condensates $\overline{D}$ (black line) and grid-mean large-scale net condensation rate $\overline{Q}$ (color) along 20°S during SON from (a, b) UNICON, (c, d) NoAdc, (e, f) P2014, (g, h) CAM5. In the Figure 8a, we also plotted A_{dc} with black-dashed lines. In each Figure 8a thick solid black line denotes the simulated PBL height.

layer within the PBL as can be seen from θ and M.

A notable difference is that, consistent with Figure 3, UNICON simulates the farthest downstream stratocumulus deck identified by the line of $A_{tot} = 0.1$ on the east of 120°W above 900 [hPa]. The budget analysis indicates that even though UNICON simulates weaker convective detrainment rates than CAM5, it simulates weaker net evaporation rates than CAM5 and P2014 due to the allocation of detrained convective condensates into the newly diagnosed detrained cumulus instead of instantaneously evaporating detrained convective condensates. As a result, the stratocumulus deck in UNICON can be sustained further downstream, resulting in the increase of CLDLOW and the improved simulation of SWCF in the downstream portion of the trade cumulus regime, as shown in Figure 3. Comparing Figures 8a and 8b with Figures 8c and 8d, the downstream extension of the stratocumulus deck in the UNICON simulation is clearly associated with the newly diagnosed detrained cumulus fraction (A_{dc}) and the resulting weaker evaporation of detrained convective condensate. A tuning effort to increase the stratus fraction by reducing critical RH slightly helps to extend the stratocumulus deck further downstream (compare Figure 9e with Figure 9c), but with a strong net evaporation rate, it is less effective than diagnosing additional detrained cumulus.

3.6. Atmospheric Variability: Diurnal Cycle of Precipitation, MJO, and the Kelvin Wave
Figure 9 shows the diurnal cycle of surface precipitation during June, July, and August, and the symmetric component of the
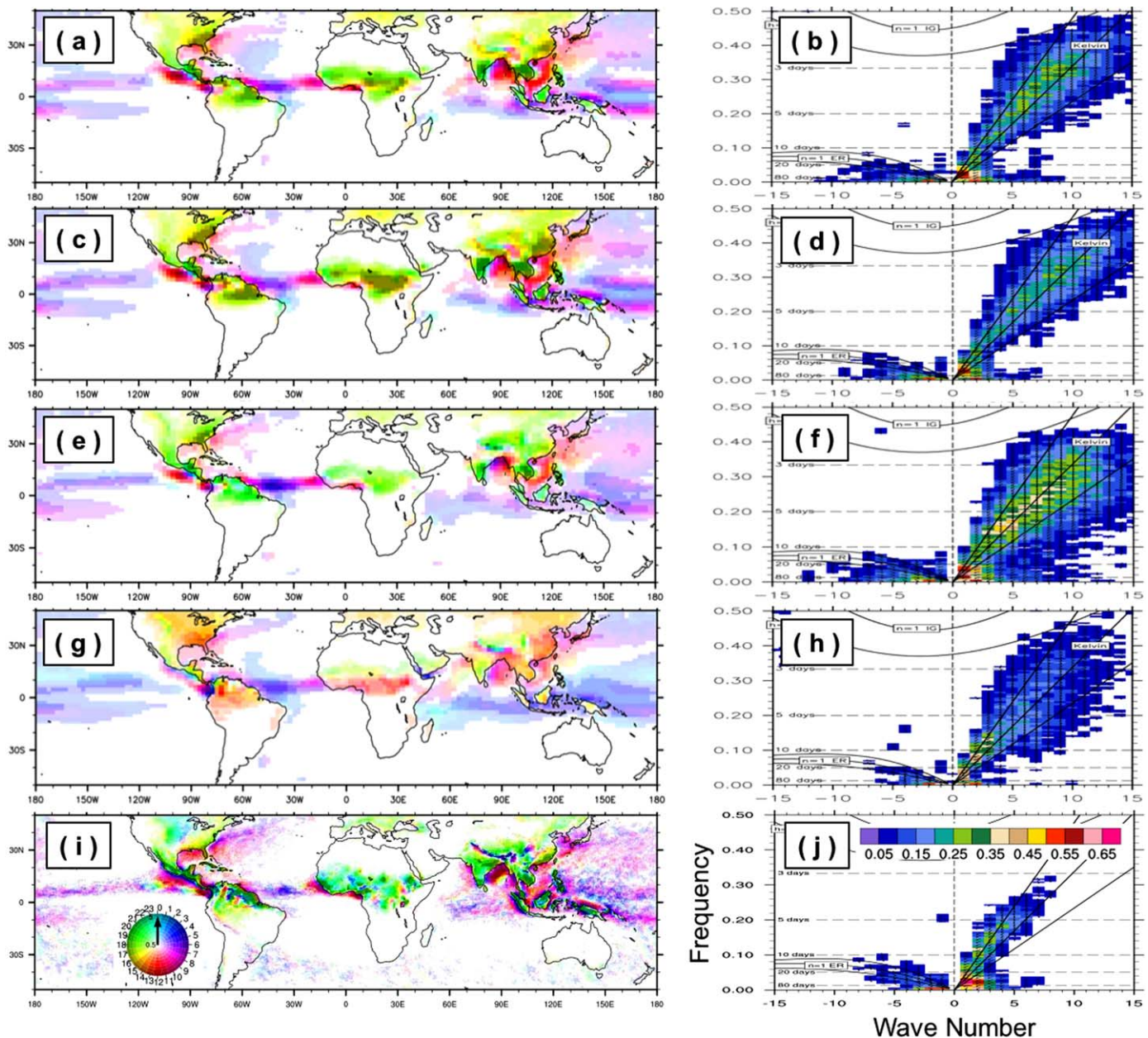
Figure 9. (left) The diurnal cycle of the total precipitation rate at the surface during JJA from (a) UNICON, (c) NoAdc, (e) P2014, (g) CAM5, and (i) the TRMM satellite observation during 2000–2009. The color scale denotes the local hour when the surface precipitation rate is at maximum and the color scale denotes the amplitude of the diurnal cycle in millimeters per day, as indicated in Figure 9i. (right) The symmetric component of coherence squared in the wavenumber-frequency space obtained from the cross-spectrum analysis of daily anomalies of OLR and zonal wind at 850 hPa in the latitude band between 15°S and 15°N for all seasons from (b) UNICON, (d) NoAdc, (f) P2014, (h) CAM5, and (f) the AVHRR satellite observation and the NCEP-NCAR reanalysis during 1979–2005.

coherence squared between the daily anomalies of outgoing longwave radiation (OLR) and zonal wind at 850 hPa (U850) in the latitude band between 15°S and 15°N from various simulations and observations. In the diurnal cycle plots, different colors denote the local hour with the maximum surface precipitation and darker shading denotes a larger amplitude of the diurnal cycle. In terms of both the time and magnitude, UNICON, NoAdc, and P2014 all well reproduce the observed peaks of the surface precipitation during the late afternoon (early morning) over the summer continents (oceans), much better than CAM5. Over the continents, the phase of the diurnal cycle simulated by UNICON (Figure 9a) is roughly similar to that of NoAdc (Figure 9c) but the amplitude is slightly reduced. This implies that detrained cumulus suppresses deep
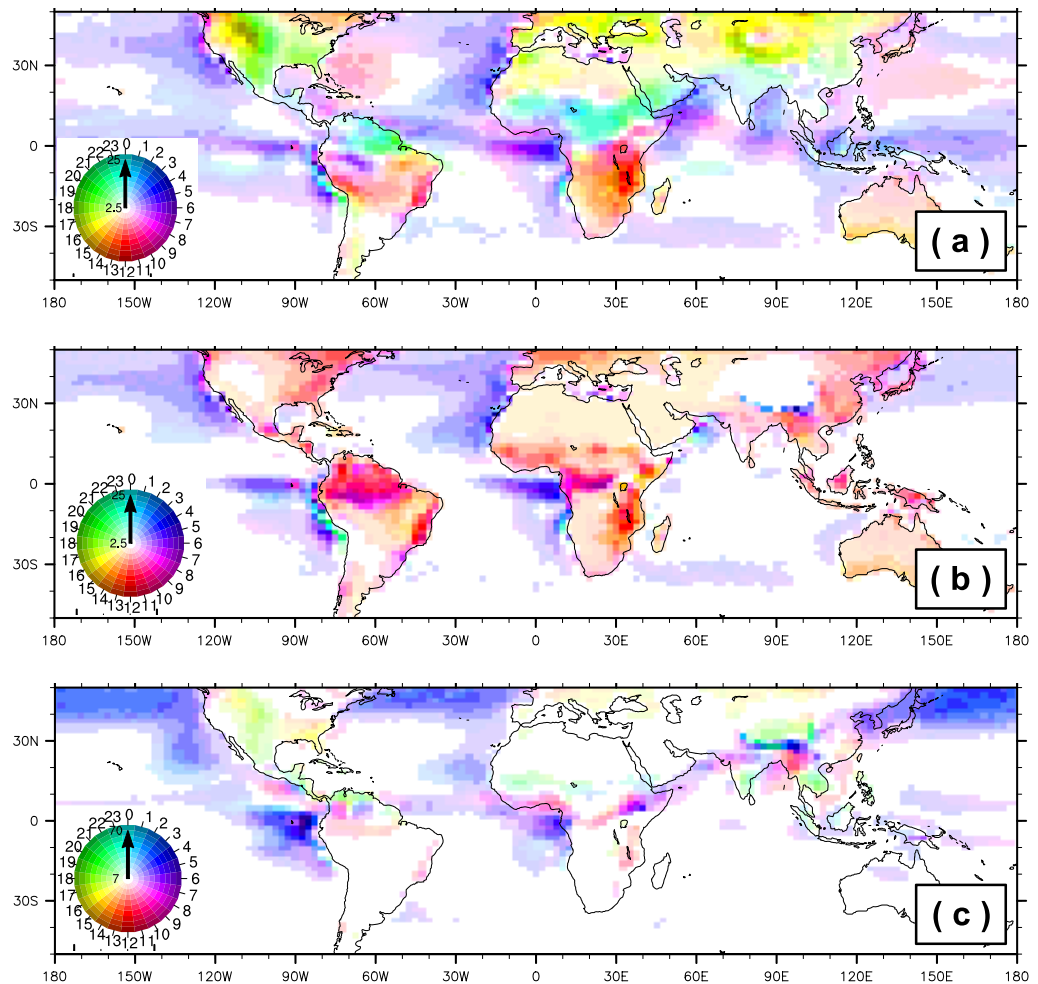
Figure 10. The diurnal cycle of (a) total cloud fraction (CLDTOT), (b) low-level cloud fraction (CLDLOW), and (c) TGCLDLWP+TGCLDIWP during JJA from UNICON. The color scale denotes the local hour when the cloud fraction is at maximum and the color scale denotes the amplitude of the diurnal cycle in units of Figures 10a and 10b (%) and Figure 10c (g · m^{-2}).

convective activity by reflecting incoming SW radiation and cooling down the surface, which may also lead to the improved simulation of climatological land rainfall with a reduced standardized deviation from NoAdc to UNICON (Figure 2).

UNICON also well reproduces the observed strong coherency between OLR and U850 for a period of 30–80 days in association with the MJO without degrading the Kelvin wave, which is a substantial improvement from CAM5. In contrast to the diurnal cycle of precipitation, the addition of detrained cumulus from NoAdc to UNICON slightly enhances the variability of the MJO and the Kelvin wave. Compared with P2014, the revised treatment of detrained convective condensates in the UNICON simulation substantially reduced noises of the coherence squared.

Figure 10 shows the UNICON-simulated diurnal cycle of total cloud fraction (CLDTOT), CLDLOW, and column-integrated grid-mean condensate water path during JJA. In the marine stratocumulus deck over the eastern subtropical and midlatitude oceans, cloud fractions and condensate water path are maximum during the night before sunrise, which is consistent with the observation [*Rozendaal et al.*, 1995]. Over the continents, the diurnal phase of CLDLOW is maximum at around noon; however, CLDTOT tends to follow or slightly lag the phase of surface precipitation during summer. Both NoAdc and P2014 simulations produce qualitatively similar results as UNICON (not shown).

4. Summary and Conclusion

A revised treatment of detrained convective condensates is combined with UNICON and tested within the CAM5 framework. The key ingredient is to diagnose a new cloud fraction (detrained cumulus) as a function of the amount of detrained convective condensates and the environmental relative humidity, instead of instantaneously evaporating convective liquids detrained into the clear portion. By construction, the detrained cumulus is not empty (i.e., it has a nonzero internal condensate mass) and is horizontally nonoverlapped with the preexisting cumulus and stratus. The implementation of detrained cumulus improved the global performance of UNICON with the largest improvement in SWCF, particularly in the downstream portion of the subtropical marine stratocumulus deck. The budget analysis indicates that although CAM5 simulates stronger convective detrainment rates, UNICON simulates weaker net evaporation rates than CAM5. This is because of the allocation of detrained convective condensates to the newly diagnosed detrained cumulus fraction, instead of evaporating convective liquids detrained into the clear portion. Further, this results in downstream extension of the marine stratocumulus deck similar to the observation. In addition to the overall mean climate, successful simulations of various atmospheric variabilities–the diurnal cycle of precipitation, MJO, and the Kelvin wave–are also well maintained. We note that compared to CAM5, UNICON substantially improves the simulations of global tropical cyclones and various aspects of the Arctic cloud system, which will be reported in separate papers. Further research is on-going to develop a comprehensive cloud scheme taking into account various aspects of individual cumulus, stratus, and detrained cumulus, including subgrid variabilities, vertical cloud overlaps, and interactions with other physical processes, such as radiation, cloud microphysics, and aerosol wet deposition.

References

Bony, S., and J.-L. Dufresne (2005), Marine boundary layer clouds at the heart of tropical cloud feedback uncertainties in climate models, *Geophys. Res. Lett.*, *32*, L20806, doi:10.1029/2005GL023851.

Hahn, C. J., and S. G. Warren (1999), *Extended Edited Synoptic Cloud Reports From Ships and Land Stations Over the Globe, 1952–1996*, Environ. Sci. Div., Off. of Biol. and Environ. Res., U.S. Dep. of Energy, 71 pp., Oak Ridge National Laboratory, Oak Ridge, TN.

Hartmann, D. L., and M. L. Michelsen (2002), No evidence for iris, *Bull. Am. Meteorol. Soc.*, *83*(2), 249.

Hwang, Y.-T., and D. M. Frierson (2013), Link between the double-intertropical convergence zone problem and cloud biases over the southern ocean, *Proc. Natl. Acad. Sci. U. S. A.*, *110*(13), 4935–4940.

Lindzen, R. S., M.-D. Chou, and A. Y. Hou (2001), Does the earth have an adaptive infrared iris?, *Bull. Am. Meteorol. Soc.*, *82*(3), 417–432.

Madden, R. A., and P. R. Julian (1971), Detection of a 40–50 day oscillation in the zonal wind in the tropical pacific, *J. Atmos. Sci.*, *28*(5), 702–708.

Medeiros, B., B. Stevens, I. M. Held, M. Zhao, D. L. Williamson, J. G. Olson, and C. S. Bretherton (2008), Aquaplanets, climate sensitivity, and low clouds, *J. Clim.*, *21*(19), 4974–4991.

Norris, J. R. (1998), Low cloud type over the ocean from surface observations. Part II: Geographical and seasonal variations, *J. Clim.*, *11*(3), 383–403.

Park, S. (2014a), A unified convection scheme (UNICON): Part I: Formulation, *J. Atmos. Sci.*, *71*(11), 3902–3930.

Park, S. (2014b), A unified convection scheme (UNICON): Part II: Simulation, *J. Atmos. Sci.*, *71*(11), 3931–3973.

Park, S., and C. S. Bretherton (2009), The University of Washington shallow convection and moist turbulence schemes and their impact on climate simulations with the Community Atmosphere Model, *J. Clim.*, *22*(12), 3449–3469.

Park, S., and C. B. Leovy (2004), Marine low-cloud anomalies associated with ENSO, *J. Clim.*, *17*(17), 3448–3469.

Park, S., C. Deser, and M. A. Alexander (2005), Estimation of the surface heat flux response to sea surface temperature anomalies over the global oceans, *J. Clim.*, *18*(21), 4582–4599.

Park, S., M. A. Alexander, and C. Deser (2006), The impact of cloud radiative feedback, remote ENSO forcing, and entrainment on the persistence of north pacific sea surface temperature anomalies, *J. Clim.*, *19*(23), 6243–6261.

Park, S., C. S. Bretherton, and P. J. Rasch (2014), Integrating cloud processes in the community atmosphere model, version 5, *J. Clim.*, *27*(18), 6821–6856.

Ramanathan, V., and W. Collins (1991), Thermodynamic regulation of ocean warming by cirrus clouds deduced from observations, *Nature*, *351*, 2.

Ramanathan, V., R. Cess, E. Harrison, P. Minnis, B. Barkstrom, E. Ahmed, and D. Hartmann (1989), Cloud-radiative forcing and climate: Results from the earth radiation budget experiment, *Science*, *243*(4887), 5763.

Rozendaal, M. A., C. B. Leovy, and S. A. Klein (1995), An observational study of diurnal variations of marine stratiform cloud, *J. Clim.*, *8*(7), 1795–1809.

Smith, R. (1990), A scheme for predicting layer clouds and their water content in a general circulation model, *Q. J. R. Meteorol. Soc.*, *116*(492), 435–460.

Taylor, K. E. (2001), Summarizing multiple aspects of model performance in a single diagram, *J. Geophys. Res.*, *106*(D7), 7183–7192.

Teixeira, J., and Y.-J. Kim (2008), On a simple parameterization of convective cloud fraction, *Asia-Pac. J. Atmos. Sci.*, *44*(2), 191–199.

Tiedtke, M. (1993), Representation of clouds in large-scale models, *Mon. Weather Rev.*, *121*(11), 3040–3061.

WMO (1975), Manual on the observation of clouds and other meteors: Volume I, WMO Publ. 407, 155 pp.

Zhang, G. J., and N. A. McFarlane (1995), Sensitivity of climate simulations to the parameterization of cumulus convection in the Canadian climate centre general circulation model, *Atmos. Ocean*, *33*(3), 407–446.